Journal of Southeast University (English Edition) Vol. 24, No. 2, pp. 183 – 187 June 2008 ISSN 1003—7985

Kinematics and dynamics analysis of a 3-7R parallel decoupling mechanism

Zheng Jianyong[1] Shi Jinfei[1] Zhang Zhisheng[1] Li Weimin[2]

([1]School of Mechanical Engineering, Southeast University, Nanjing 211189, China)

([2]School of Mechanical Engineering, Hebei University of Technology, Tianjin 300130, China)

Abstract: One kind of movable-pair analysis method is adopted to analyze the configuration of a 3-7R (revolute-pair) parallel decoupling mechanism, and the mechanism's characteristics are summarized. The mechanism has three orthogonal distributional branch-chains, and all movable pairs are rotational joints. The movable platform of the mechanism has x, y, z translational decoupling directions. Furthermore, in order to verify the mechanism's decoupling characteristics, the mechanism's kinematics analysis is solved, and the mechanism's direct/inverse kinematics model, input/output velocities and accelerations are deduced, which confirm its decoupling movement characteristics. Finally, one kind of mechanism link decomposed-integrated approach is adopted, and the mechanism's dynamics model is completed with the Lagrange method, which also proves its decoupling force characteristics. All of these works provide significant theory for the further study of the mechanism's control strategy, design, path planning etc.

Key words: 3-7R parallel decoupling mechanism; kinematics; dynamics; decoupling

The 3-DOF(degrees of freedom) parallel robot has good practical prospects in the parallel robot application areas[1] and it is also a hot-spot. Gosselin and Angeles[2-3] proposed plane, spherical 3-DOF parallel robot design optimization. Lee and Shah[4] studied the 3-DOF parallel robot's design. Hunt[5] proposed a three-degree of freedom 3-RPS space parallel mechanism. Jin and Yang[6-7] analyzed one novel three translational decoupling parallel mechanism. Based on the theory of mechanism structure, Li et al.[8] synthesized out one kind of absolute decoupling 3-DOF parallel mechanism, which has one pure-translation pair and two revolute pairs. Furthermore, based on decoupling determination criteria, Hang et al.[9] suggested a novel decoupling parallel mechanism, which has three pure-translation pairs and one revolute pair; in addition, this mechanism has both the topological decoupling and the criteria decoupling characteristics. In view of the basic principles of translational decoupling mechanisms, the configuration characteristics of a 3-7R(revolute pair) parallel mechanism[10-11] are proposed in this paper. Furthermore, the mechanism's kinematics and dynamics analyses are carried out, which proves the mechanism's movement and force decoupling characteristics. All of these works provide significant theory for the further study of the mechanism's control strategy, promotion applications etc.

Received 2007-11-23.

Biographies: Zheng Jianyong (1978—), male, graduate; Shi Jinfei (corresponding author), male, doctor, professor, shijf@seu.edu.cn.

Foundation item: The National High Technology Research and Development Program of China(863 Program) (No. 2006AA040202).

Citation: Zheng Jianyong, Shi Jinfei, Zhang Zhisheng, et al. Kinematics and dynamics analysis of a 3-7R parallel decoupling mechanism[J]. Journal of Southeast University (English Edition), 2008, 24(2): 183 – 187.

1 Configuration Analysis and Characteristics

The basic idea of the translational decoupling configuration is: A linear movement input is irrelevant to the perpendicular motion which is in the plane input. The physical meaning of the idea is shown in Fig. 1(a). The prismatic pair P is identified as a motion input, which can determine the location of a z-coordinate axis direction. Otherwise, the movement of the plane pair F along x, y directions is irrelevant to P. Thus, as shown in Fig. 1(a), the motion's diagram is a defined branch chain PF, which can form the input/output corresponding translational decoupling parallel mechanism.

If the branched-chain PF is further studied, a new 7R (revolute-pair) branched-chain can be designed as shown in Fig. 1(b). The parallelogram mechanism is defined as P and the two-linking rods represent plane F. Furthermore, three 7R branches can combine the 3-7R parallel decoupling mechanism(see Fig. 2), and its characteristics are as follows:

1) Having a simple structure, and all the movement pairs of the mechanism are rotational joints.

2) Having servo motors that can be used for the mechanism's drive energy, which has a simple control-pattern.

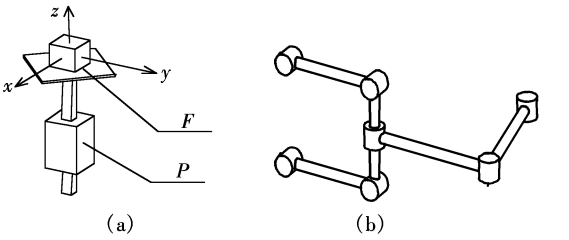

Fig. 1 Configuration research of parallel mechanism decoupling. (a) Movement sketch of P and F; (b) 7R branch

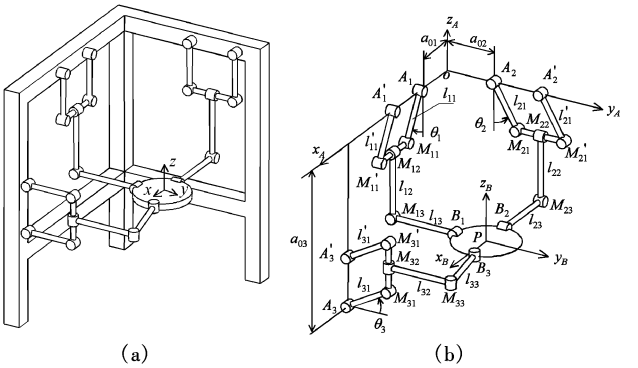

Fig. 2 Three degree of freedom parallel mechanism

3) Connecting with the stable platform, the pairs are in spatial orthogonal distribution, and each branch movement separately controls one direction of the movable platform.

4) Connecting with the movable platform, the axis of the revolute pair is in a spatial orthogonal direction, which can overcome the general coupling defects of the parallel mechanism.

5) Having some other characteristics, such as movement/strength decoupling, continuous work space, simple assembly process and so on.

2 Kinematics Analysis

2.1 Coordinate establishment

Let $o\text{-}x_A y_A z_A$ be a fixed coordinate system, which is in the top left of the mechanical rack. However, the movable coordinate system $P\text{-}x_B y_B z_B$ is installed in the geometric center of the movable platform. In the following, the value of the subscript $i = 1, 2, 3$. Then, parameter β_i is defined as the angle between $M_{i1}M_{i3}$ and its corresponding coordinate axis. Parameter β_i' stands for the angle between $M_{i3}B_i$ and corresponding axis. The parameters m_{0i} represent the rod length of $M_{i1}M_{i1}'$, and the other parameter definitions are shown in Fig. 2.

$$\left\{\begin{array}{c} a_{01} + l_{11}\sin\theta_1 + m_{01} \\ l_{12}\sin\beta_1 + l_{13}\cos(\beta_1' + \beta_1) \\ l_{11}\cos\theta_1 + l_{12}\cos\beta_1 + l_{13}\sin(\beta_1' + \beta_1) \end{array}\right\} = \left\{\begin{array}{c} X_P \\ Y_P - r \\ Z_P \end{array}\right\} \tag{1}$$

$$\left\{\begin{array}{c} l_{22}\sin\beta_2 + l_{23}\cos(\beta_2 + \beta_2') \\ a_{02} + l_{21}\sin\theta_2 + m_{02} \\ l_{21}\cos\theta_2 + l_{22}\cos\beta_2 + l_{23}\sin(\beta_2 + \beta_2') \end{array}\right\} = \left\{\begin{array}{c} X_P - r \\ Y_P \\ Z_P \end{array}\right\} \tag{2}$$

$$\left[\begin{array}{c} a_{04} - [l_{32}\sin\beta_3 + l_{33}\cos(\beta_3 + \beta_3')] \\ l_{31}\cos\theta_3 + l_{32}\cos\beta_3 + l_{33}\sin(\beta_3 + \beta_3') \\ -a_{03} + l_{31}\sin\theta_3 + m_{03} \end{array}\right] = \left\{\begin{array}{c} X_P + r \\ Y_P \\ Z_P \end{array}\right\} \tag{3}$$

2.2 Inverse kinematics problem

1) Solution of the input variables

$$\left.\begin{array}{l} \theta_1 = \arcsin\left(\dfrac{X_P - m_{01} - a_{01}}{l_{11}}\right) \\ \theta_2 = \arcsin\left(\dfrac{Y_P - m_{02} - a_{02})}{l_{21}}\right) \\ \theta_3 = \arcsin\left(\dfrac{Z_P - m_{03} + a_{03})}{l_{31}}\right) \end{array}\right\} \tag{4}$$

2) Solution of the intermediate variables

$$\beta_1 = \arctan\left(\frac{-UV \pm \sqrt{U^2V^2 - (V^2 - D^2)(U^2 - D^2)}}{(U^2 - D^2)}\right) \tag{5}$$

$$\beta_2 = \arctan\left(\frac{-U'V' \pm \sqrt{U'^2V'^2 - (V'^2 - D'^2)(U'^2 - D'^2)}}{(U'^2 - D'^2)}\right) \tag{6}$$

$$\beta_3 = \arctan\left(\frac{-U''V'' \pm \sqrt{U''^2V''^2 - (V''^2 - D''^2)(U''^2 - D''^2)}}{(U''^2 - D''^2)}\right) \tag{7}$$

where

$$D = \frac{(Y_P - r)^2 + (Z_P - l_{11}\cos\theta_1)^2 + l_{12}^2 - l_{13}^2}{/2l_{12}}$$

$$U = Y_P - r,\ V = Z_P - l_{11}\cos\theta_1,\ U' = X_P - r,\ V' = Z_P - l_{21}\cos\theta_2$$

$$\beta_1' = \arctan\left(\frac{Z_P - l_{11}\cos\theta_1 - l_{12}\cos\beta_1}{Y_P - r - l_{12}\sin\beta_1}\right) - \beta_1$$

$$D' = \frac{(X_P - r)^2 + (Z_P - l_{21}\cos\theta_2)^2 + l_{22}^2 - l_{23}^2}{2l_{22}}$$

$$\beta_2' = \arctan\left(\frac{Z_P - l_{21}\cos\theta_2 - l_{22}\cos\beta_2}{X_P - r - l_{22}\sin\beta_2}\right) - \beta_2$$

$$D'' = \frac{(a_{04} - X_P - r)^2 + (Y_P - l_{31}\cos\theta_3)^2 + l_{32}^2 - l_{33}^2}{2l_{32}}$$

$$U'' = a_{04} - X_P - r, \quad V'' = Y_P - l_{31}\cos\theta_3$$

2.3 Direct kinematics problem

The direct kinematics problem is the opposite of the inverse kinematics problem of the mechanism; i. e. , if the parallel robot's structural parameters and the size(degree) of every mechanism link's input-movement-pair's angles are known in advance, then, the location reference point $P(X_P, Y_P, Z_P)$ of the movable platform of the mechanism is easy to be solved

$$\left.\begin{array}{l} X_P = a_{01} + l_{11}\sin\theta_1 + m_{01} \\ Y_P = a_{02} + l_{21}\sin\theta_2 + m_{02} \\ Z_P = -a_{03} + l_{31}\sin\theta_3 + m_{03} \end{array}\right\} \tag{8}$$

2.4 Velocities and accelerations

As for the movable platform being rigid-body, the linear platform point's velocities and accelerations are equal to each other. Therefore, it can obtain the speed of the movable platform by means of taking X_P, Y_P and Z_P to the first time of the derivative. Furthermore, the velocity's positive solution of the parallel mechanism is

$$\boldsymbol{V}_P = \{\dot{X}_P,\ \dot{Y}_P,\ \dot{Z}_P\}^{\mathrm{T}} \tag{9}$$

By further deducing to the upper formula, the inverse solution of the mechanism can be obtained.

$$\dot{\boldsymbol{\theta}} = \{\dot{\theta}_1,\ \dot{\theta}_2,\ \dot{\theta}_3\}^{\mathrm{T}} = \boldsymbol{J}^{-1}\{\dot{X}_P,\ \dot{Y}_P,\ \dot{Z}_P\}^{\mathrm{T}} \tag{10}$$

where

$$\boldsymbol{J}^{-1} = \left[\begin{array}{ccc} \dfrac{1}{l_{11}\cos\theta_1} & 0 & 0 \\ 0 & \dfrac{1}{l_{21}\cos\theta_2} & 0 \\ 0 & 0 & \dfrac{1}{l_{31}\cos\theta_3} \end{array}\right] \tag{11}$$

If some parameters, such as the mechanism's size, the velocities and the accelerations of the drive pair angles, are known in advance, every component's acceleration of the movable platform can be obtained.

$$\begin{Bmatrix}\ddot{\theta}_1\\ \ddot{\theta}_2\\ \ddot{\theta}_3\end{Bmatrix}=\boldsymbol{J}^{-1}\left(\begin{Bmatrix}\ddot{X}_P\\ \ddot{Y}_P\\ \ddot{Z}_P\end{Bmatrix}-\begin{bmatrix}-l_{11}\sin\theta_1 & 0 & 0\\ 0 & -l_{21}\sin\theta_2 & 0\\ 0 & 0 & -l_{31}\sin\theta_3\end{bmatrix}\begin{Bmatrix}\dot{\theta}_1^2\\ \dot{\theta}_2^2\\ \dot{\theta}_3^2\end{Bmatrix}\right) \tag{12}$$

Therefore, according to the decoupling configuration idea of the translational parallel mechanism, then, the 3-7R parallel mechanism has movement decoupling characteristics, and its every branch is in one to one correspondence decoupling.

3 Parallelogram Mechanism Static Analysis

As it is known, the parallelogram mechanism is a statically indeterminate structure. In order to overcome the statically indeterminate structure's defects, the servo motor is assumed to be installed in the bottom joint of the parallelogram mechanism, which can provide a balance moment for the parallelogram mechanism to be a static spatial mechanism. Known by the principle of virtual work, there is a balance condition to the particle system, which is in the ideal constraint circumstance. That is to say, the virtual works equal zero, which is initially done by the particle system in any virtual displacement. The parallelogram mechanism's virtual displacement diagram is shown in Fig. 3; the input torque of each branch is defined M_i, and the 4th link of each branch's internal strength in the point M_{i2} is replaced by f'_{41}. The relationship of M_i and f'_{41} is completed as

$$\left.\begin{aligned}M_1&=f_{41}^1\ l'_{11}\cos\theta_1=P_X\ l'_{11}\cos\theta_1\\ M_2&=f_{41}^2\ l'_{21}\cos\theta_2=P_Y\ l'_{21}\cos\theta_2\\ M_3&=f_{41}^3\ l'_{31}\cos\theta_3=P_Z\ l'_{31}\cos\theta_3\end{aligned}\right\} \tag{13}$$

Eq. (13) can be written in the matrix form:

$$\begin{Bmatrix}P_1\\ P_2\\ P_3\end{Bmatrix}=\begin{bmatrix}\dfrac{1}{l'_{11}\ cos\theta_1} & 0 & 0\\ 0 & \dfrac{1}{l'_{21}\cos\theta_2} & 0\\ 0 & 0 & \dfrac{1}{l'_{31}\cos\theta_3}\end{bmatrix}\begin{Bmatrix}M_1\\ M_2\\ M_3\end{Bmatrix} \tag{14}$$

In addition, if the generalized driving-force is replaced by $\boldsymbol{P}$, and $\boldsymbol{M}$ substitutes for the driving torque of the servo motor, the relationship of $\boldsymbol{P}$ and $\boldsymbol{M}$ is $\boldsymbol{P}=\boldsymbol{GM}$, where

$$\boldsymbol{G}=\begin{bmatrix}\dfrac{1}{l'_{11}\cos\theta_1} & 0 & 0\\ 0 & \dfrac{1}{l'_{21}\cos\theta_2} & 0\\ 0 & 0 & \dfrac{1}{l'_{31}\cos\theta_3}\end{bmatrix} \tag{15}$$

Furthermore, $\boldsymbol{G}$ is also defined as the power transfer matrix of the parallelogram mechanism, i. e. the power Jacobian matrix, which conforms to the antithesis relations of the movement and strength transmission. On the other hand, the following formula $l'_{i1}=l_{i1}$ is known (see Fig. 2), so the further formula is $\boldsymbol{G}=\boldsymbol{J}^{-1}$.

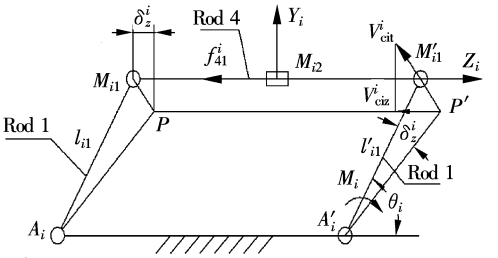

Fig. 3 Parallelogram mechanism's virtual displacement

4 Dynamics Analysis

The establishment of the parallel robot dynamics model is the basis for the robot's control. Furthermore, the accuracy of dynamics model determines the parallel robot's control accuracy. The Lagrange method is adopted to establish 3-7R parallel mechanism dynamics model in this paper. Once the spatial tracks of the robot's joint variables have been identified, or the track of the robot's end effectors has been determined in the Descartes coordinate (i. e. the motion paths have been planned), then, the solution of each robot actuator's driving force/torque is defined as a reverse dynamics problem. Knowing from the 3-7R parallel mechanism's kinematics analysis, each branched-chain's motion is decoupled, and the change of θ_i can only cause the movable platform to move along the corresponding X, Y, Z translation directions. Therefore, the inverse dynamics model of the 3-7R parallel mechanism is to establish the relationship of M_i and θ_i ($i=1, 2, 3$). Therefore, M_i is defined as the driving torque of the parallelogram mechanism bottom's rotational joint $A_i(A'_i)$, and θ_i stands for the pendulum angle of the parallelogram mechanism. Then, let each 3-7R parallel mechanism's component be a part of the generalized force, and by the Lagrange method, the parallel mechanism's inverse dynamics model can be solved.

4.1 Establishment of link-rod coordinate

As shown in Fig. 4, joint M_{i2} is selected to stand for the origin of an absolute coordinate system. In addition, Q_1 and Q_2 are defined as the two link rod's centroid, and r_1 and R_{21} (the absolute coordinate vector) determine the values of Q_1 and Q_2. R_{21} depends on each rod's generalized coordinate posture. In order to identify the position of the Q_1 and Q_2 centroid, then, the following terms are defined.

T_i is the homogeneous coordinate transformation of coordinate $i(1, 2)$ to the absolute coordinate system; $\tilde{r}_i$ is the variable in the $i(1, 2)$ coordinate system; e_i is the unit variable of each rod coordinate system, which is described by the absolute coordinate; r_1 is the position variable of the centroid Q_1; R_{21} is the position variable of the centroid Q_2.

Furthermore, the following formula can interpret the relationship of these parameters[12].

$$Q_1: r_1=T_1\tilde{r}_1;\ Q_2:\quad R_{21}=T_1\tilde{r}_1-T_1\tilde{R}_1+T_2\tilde{r}_2 \tag{16}$$

4.2 Solution of general driving torque

In the following formula, $\boldsymbol{U}_i$ is defined as the none-driv-

ing force of the link-rod system, and P_i stands for the joint's general driving torque. Some parameters are also defined as follows: $S_1 = \sin\beta_i$, $S_2 = \sin\beta'_i$, $C_1 = \cos\beta_i$, $C_2 = \cos\beta'_i$.

$$\boldsymbol{U}_i = \dot{\boldsymbol{M}}\dot{\boldsymbol{q}} - \frac{1}{2}\dot{\boldsymbol{q}}^{\mathrm{T}}\frac{\partial \boldsymbol{M}}{\partial \boldsymbol{q}}\dot{\boldsymbol{q}} - \boldsymbol{Y} = \begin{Bmatrix} (m_1+m_2)gl_{i2}C_1 + m_2gl_{i3}C_2 \\ m_2gl_{i3}C_2 \end{Bmatrix} + \begin{Bmatrix} -m_2l_{i2}l_{i3}S_2\dot{\beta}'^2_i - 2m_2l_{i2}l_{i3}S_2\dot{\beta}_i\dot{\beta}'_i \\ m_2l_{i2}l_{i3}\dot{\beta}^2_i \end{Bmatrix} \tag{17}$$

$$\boldsymbol{P}_i = \boldsymbol{M}\ddot{\boldsymbol{q}} + \boldsymbol{U}_i = \begin{Bmatrix} \tau_1 \\ \tau_2 \end{Bmatrix} = \begin{Bmatrix} (m_1+m_2)gl_{i2}C_1 + m_2gl_{i3}C_2 \\ m_2gl_{i3}C_2 \end{Bmatrix} + \begin{Bmatrix} m_2l_{i3}^2 + 2m_2l_{i2}l_{i3}C_2 + (m_1+m_2)l_{i2}^2 & m_2l_{i2}l_{i3}C_2 + m_2l_{i3}^2 \\ m_2l_{i2}l_{i3}C_2 + m_2l_{i3}^2 & m_2l_{i3}^2 \end{Bmatrix} \begin{Bmatrix} \ddot{\beta}_i \\ \ddot{\beta}'_i \end{Bmatrix} + \begin{Bmatrix} -m_2l_{i2}l_{i3}S_2\dot{\beta}'^2_i - 2m_2l_{i2}l_{i3}S_2\dot{\beta}_i\dot{\beta}'_i \\ m_2l_{i2}l_{i3}S_2\dot{\beta}^2_i \end{Bmatrix} \tag{18}$$

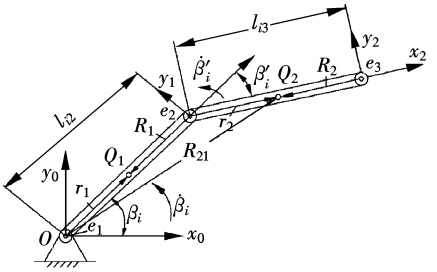

Fig. 4 Coordinates of the link-rod system

4.3 Dynamic model of 3-7R parallel mechanism

In order to conveniently express the model of the 3-7R parallel mechanism and to find the law in the complicated analytic formula of the mechanism's dynamic model, some equations and parameters are defined as follows:

$$T_1 = m_2l_{i3}^2 + 2m_2l_{i2}l_{i3}C_2 + (m_1+m_2)l_{i2}^2$$
$$T_2 = m_2l_{i2}l_{i3}C_2 + m_2l_{i3}^2, \quad T_3 = m_2l_{i3}^2$$
$$T_4 = -m_2l_{i2}l_{i3}S_2\dot{\beta}'^2_i - 2m_2l_{i2}l_{i3}S_2\dot{\beta}_i\dot{\beta}'_i$$
$$T_5 = m_2l_{i2}l_{i3}S_2\dot{\beta}^2_i$$
$$T_6 = (m_1+m_2)gl_{i2}C_1 + m_2gl_{i3}C_2$$
$$T_7 = m_2gl_{i3}C_2$$

Furthermore, after the reorganization of Eq. (18), we can obtain the following result:

$$\boldsymbol{P}_i = \boldsymbol{M}\ddot{\boldsymbol{q}} + \boldsymbol{U}_i = \begin{Bmatrix} \tau_1 \\ \tau_2 \end{Bmatrix} = \begin{bmatrix} T_1 & T_2 \\ T_2 & T_3 \end{bmatrix}\begin{Bmatrix} \ddot{\beta}_i \\ \ddot{\beta}'_i \end{Bmatrix} + \begin{Bmatrix} T_4 \\ T_5 \end{Bmatrix} + \begin{Bmatrix} T_6 \\ T_7 \end{Bmatrix} = \begin{Bmatrix} T_1\ddot{\beta}_i + T_2\ddot{\beta}'_i \\ T_2\ddot{\beta}_i + T_3\ddot{\beta}'_i \end{Bmatrix} + \begin{Bmatrix} T_4 + T_6 \\ T_5 + T_7 \end{Bmatrix} = \begin{Bmatrix} T_1\ddot{\beta}_i + T_2\ddot{\beta}'_i + T_4 + T_6 \\ T_2\ddot{\beta}_i + T_3\ddot{\beta}'_i + T_5 + T_7 \end{Bmatrix} \tag{19}$$

Therefore, we can obtain the following equation from $\boldsymbol{M} = \boldsymbol{G}^{-1}\boldsymbol{P} = [\boldsymbol{J}^{-1}]^{-1}\boldsymbol{P} = \boldsymbol{J}\boldsymbol{P}$.

$$\begin{bmatrix} M_1 \\ M_2 \\ M_3 \end{bmatrix} = \boldsymbol{J}\begin{Bmatrix} P_1 \\ P_2 \\ P_3 \end{Bmatrix} = \begin{bmatrix} l_{11}\cos\theta_1 & 0 & 0 \\ 0 & l_{21}\cos\theta_2 & 0 \\ 0 & 0 & l_{31}\cos\theta_3 \end{bmatrix}\begin{Bmatrix} P_1 \\ P_2 \\ P_3 \end{Bmatrix} = \begin{Bmatrix} l_{11}\cos\theta_1P_1 \\ l_{21}\cos\theta_2P_2 \\ l_{31}\cos\theta_3P_3 \end{Bmatrix}$$

That is

$$M_i = l_{i1}\cos\theta_iP_i \tag{20}$$

From Eq. (20), M_i and θ_i are only related to each corresponding parameter, and are independent of the other parameters. Therefore, we can draw the conclusion concerning the 3-7R parallel mechanism's force decoupling.

5 Conclusion

Based on the analysis of the movable pair, the configuration analysis of a 3-7R (revolute pair) parallel decoupling mechanism is presented and the parallel mechanism's characteristics are summarized. Furthermore, kinematics analysis of the 3-7R parallel decoupling mechanism is also solved, and the mechanism's direct/inverse kinematics, input/output velocities and accelerations are deduced, which confirms the mechanism's kinematics decoupling characteristics. In addition, based on the results of kinematics analysis and virtual work theory, parallelogram mechanism's static analyses are performed. Finally, the Lagrange method is adopted to establish the dynamics model of the 3-7R parallel mechanism, which proves the mechanism's force decoupling characteristics. All the analyses will be the base of further study on the mechanism's control strategy and the design.

References

[1] Cao Yanxia. The study of the decoupled force feedback manipulator with 3-DOF translation [D]. Tianjin: School of Mechanical Engineering of Hebei University of Technology, 2004. (in Chinese)

[2] Gosselin C M, Angeles J. The optimum kinematic design of a planar three-degree-of-freedom parallel manipulator [J]. *ASME J Mech Trans Autom Des*, 1988, **110**(1): 35 − 41.

[3] Gosselin C M, Angeles J. The optimum kinematic design of a spherical three-degree-of-freedom parallel manipulator [J]. *ASME J Mech Trans Autom Des*, 1989, **111**(2): 202 − 207.

[4] Lee K M, Shah D K. Kinematic analysis of a three-degree-of-freedom parallel actuated manipulator [J]. *IEEE Journal of Robotics and Automation*, 1988, **4**(3): 354 − 360.

[5] Hunt K H. Structural kinematics of in-actuated robot-arms [J]. *ASME J Mech Trans Autom Des*, 1983, **105**(4): 705 − 712.

[6] Jin Qiong, Yang Tingli. Position analysis for a class of novel 3-DOF translational parallel robot mechanisms[J]. *Journal of Southeast University*: *Natural Science Edition*, 2001, **31**(5): 33 − 38. (in Chinese)

[7] Jin Qiong, Yang Tingli. Synthesis and analysis of a group of 3-degree-of-freedom partially decoupled parallel manipulators [J]. *Journal of Mechanical Design*, 2004, **126**(2): 301 − 306.

[8] Li Huiliang, Jin Qiong, Yang Tingli. A group of 3-DOF decoupled parallel mechanisms and their displacement analyses [J]. *Machine Building & Automation*, 2002(1): 9 − 14. (in Chinese)

[9] Hang Lubin, Wang Yan, Yang Tingli. Analysis of a new type 3 translations-1 rotation decoupled parallel manipulator[J]. *China Mechanical Engineering*, 2004, **15**(12): 1035 − 1037; 1041. (in Chinese)

[10] Li Weimin, Gao Feng, Zhang Jianjun. A three-DOF translational manipulator with decoupled geometry [J]. *Robotics*, 2005, **23**(6): 805 − 808.

[11] Li Weimin, Gao Feng, Zhang Jianjun. R-CUBE, a decoupled

parallel manipulator only with revolute joints [J]. *Mechanism and Machine Theory*, 2005, **40**(4): 467 − 473.

[12] Zhao Xifang. *Robot dynamics* [M]. Shanghai: Shanghai Jiaotong University Press, 2001. (in Chinese)

一种 3-7R 并联解耦机构的运动学与动力学分析

郑建勇[1] 史金飞[1] 张志胜[1] 李为民[2]

([1] 东南大学机械工程学院,南京 211189)

([2] 河北工业大学机械工程学院,天津 300130)

摘要:基于运动副分析,对一种运动解耦的 3-7R 并联机构进行了构型分析,并对机构的构型特点进行了总结. 该机构由 3 个正交分布的支链组成,机构的运动副均为转动副,构成了机构动平台在 x,y,z 三个方向的平动解耦. 为验证机构的解耦特性,对机构进行了运动学分析,推导了机构的运动学正/反解、输入/输出的速度和加速度,验证了机构的运动解耦特性. 采用一种机构支链分解−综合的方法,利用拉格朗日法建立了机构的动力学模型,验证了机构的力解耦特性. 这对机构控制策略、机构设计和轨迹规划等方面的研究具有一定的理论意义.

关键词:3-7R 并联解耦机构;运动学;动力学;解耦

中图分类号:TP242;TH113